Piezoelectric $K_{0.5}Na_{0.5}NbO_3$ ceramics textured using needle-like $K_{0.5}Na_{0.5}NbO_3$ templates

Astri Bjørnetun Haugen,[1] Gerhard Henning Olsen,[1] Francesco Madaro,[1] Maxim I. Morozov,[1] Goknur Tutuncu,[2] Jacob L. Jones,[2,3] Tor Grande[1] and Mari-Ann Einarsrud[1]

[1] Department of Materials Science and Engineering, Norwegian University of Science and Technology (NTNU), Trondheim, Norway

[2] Department of Materials Science and Engineering, University of Florida, Gainesville, FL, USA

[3] Department of Materials Science and Engineering, North Carolina State University, Raleigh, NC, USA

Corresponding author:
Mari-Ann Einarsrud
Mari-Ann.Einarsrud@ntnu.no

Abstract

Improved performance by texturing has become attractive in the field of lead-free ferroelectrics, but the effect depends heavily on the degree of texture, type of preferred orientation, and whether the material is a rotator or extender ferroelectric. Here we report on successful texturing of $K_{0.5}Na_{0.5}NbO_3$ (KNN) ceramics by alignment of needle-like KNN templates in a matrix of KNN powder using tape casting. Homotemplated grain growth of the needles was confirmed during sintering, resulting in a high degree of texture parallel to the tape casting direction and the aligned needles. The texture significantly improved the piezoelectric response parallel to the tape cast direction, corresponding to the direction of the strongest $<001>_{pc}$ orientation, while the response normal to the tape cast plane was lower than for a non-textured KNN. *In situ* X-ray diffraction during electric field application revealed that non-180° domain reorientation was enhanced by an order of magnitude in the tape casting direction, compared to the direction normal to the tape cast plane and in the non-textured ceramic. The effect of texture in KNN is discussed with respect to possible rotator ferroelectric properties of KNN.

Introduction

The last decade has seen a considerable effort to develop lead-free alternatives to lead zirconate titanate (PZT) based piezoelectric materials.[1,2] Several approaches to enhance the piezoelectric properties of lead-free ceramics have been investigated, generally categorized as either compositional engineering (e.g. doping) or microstructural engineering (e.g. crystallographic or grain texture).[3] Grain texture refers to the preferred orientation of the crystals in the pseudo-cubic (pc) unit cell reference frame, i.e. the grain orientation without considering spontaneous strains that are present below the Curie temperature. Grain texturing in polycrystalline ceramics moves the properties towards the properties of single crystals, allowing utilization of the inherent anisotropy of the piezoelectric constants.[4] Grain texture in which the polar axes are oriented away from the direction of the electric field is expected to increase the piezoelectric response of "rotator ferroelectrics," [5,6] while a maximized response is expected for "extender ferroelectrics" [5,6] when the grain texture orients the polar axes parallel to the electric field.

Grain texture is commonly obtained using templated grain growth (TGG).[4] In this process, anisometric template particles are aligned in a matrix phase through the shearing forces of a casting process and these templates act as nucleation sites for preferential grain growth during sintering. When the templates and matrix phase have identical composition and structure, the TGG process is said to be homoepitaxial. In contrast heteroepitaxial TGG occurs when the templates and matrix have related crystal structures but differ in composition. A complete reaction between templates and matrix is necessary when heteroepitaxial TGG is utilized for texturing, since residual template particles might impede densification and domain wall motion.[4] Moreover, in order to obtain a textured polycrystal as close to a single crystal as possible, a preferred orientation of planes in more than one direction is desired.[4]

Both compositional and microstructural engineering have been applied to $K_{0.5}Na_{0.5}NbO_3$ (KNN).[7,8] KNN is an orthorhombic (*Amm*2) perovskite at room temperature, but is commonly described with a pseudo-cubic unit cell. The piezoelectric constant, d_{33}, of conventionally sintered KNN vary from 80 to 120 pC/N with densities in the range 90-93 %.[1] $<001>_{pc}$ texture introduced by tape casting with $NaNbO_3$ platelet templates and heterotemplated grain growth resulted in a d_{33} value of 373 pC/N in Li and Ta co-doped KNN.[7] This method has been used previously to fabricate textured KNN,[9-13] and results in a fiber texture with a $<001>_{pc}$ axis normal to the tape cast plane. Ceramics prepared by lamination of such tapes with electrodes parallel to the tape cast plane therefore have the orthorhombic polar axes ($<011>_{pc}$) oriented away from the direction of the applied electric field. Although no data on KNN single crystals are readily available, piezoelectric constants for single crystal $KNbO_3$[6,14-17] and KNN ceramics[18-21] indicate that KNN is a rotator ferroelectric. High piezoelectric response in $<001>_{pc}$ textured orthorhombic KNN ceramics is therefore expected in accordance with rotator ferroelectric behavior.

In this work, we introduce a new technique for texturing of KNN by tape casting using needle-like KNN templates followed by homoepitaxial grain growth during sintering. First we demonstrate that this technique results in strong texture parallel to the tape casting direction and that an orthotropic texture is introduced due to the needle-like KNN templates, whereas prior work[9-13] using platelet $NaNbO_3$ templates have created textures of fiber symmetry. *In situ* X-ray diffraction during loading of an electrical field was used to investigate domain switching and crystallographic strain. Finally, the effect of the texture on the piezoelectric and ferroelectric properties are investigated and discussed in relation to the possible rotator ferroelectric properties of KNN.

Experimental

Submicron $K_{0.5}Na_{0.5}NbO_3$ (KNN) powder was prepared by spray pyrolysis[22,23] of an aqueous precursor solution of KNO_3, $NaNO_3$ (>99 %, Merck, Darmstadt, Germany) and $(NH_4)NbO(C_2O_4)_2\times 5H_2O$ (H.C. Starck, Goslar, Germany). KNN templates were prepared through molten salt synthesis of $K_2Nb_4O_{11}$ anisometric particles, and subsequent conversion to KNN as described elsewhere.[24,25] Textured ceramics were produced by tape casting of an aqueous slip with composition as described by Lein *et al.*[26] (Table I). The submicron KNN powder, solvent and dispersant were mixed by ball milling for 5-6 h. Binder, plasticizer and defoamer were then added and the mixing continued for another 16-24 h. The anisometric KNN template particles were added to the slip along with defoamer, stirred for 3 h and de-aired prior to tape casting.

The slip was tape cast by a Mistler Table Top Caster (TTC-1200, Richard E. Mistler, Inc., Morrisville, PA) on a Mylar™ film at a speed of 15 cm/min. In order to align the needle-like templates, the doctor blade was modified by adding vertical gates consisting of 0.5 mm separated pins as per the method developed by Park and Kim.[27] A schematic of the tape casting process showing the tape casting direction (TCD), transverse direction (TD) and the normal direction (ND) used for describing the texture is shown in Fig. 1. The tape cast plane is defined by the TCD and TD axes. After drying for ~20 h at ambient conditions, green tape cut-outs were stacked, all with their TCD in the same direction. The stacked cut-outs were laminated by hot pressing at 30 MPa for 10 min at 70 °C to produce green compacts. Organics were burnt out at 600 °C for 6 h (heating rates of 25 °C/h up to 180 °C, 12 °C/h further up to 600 °C). The compacts were sintered at 1130 °C in flowing O_2 with heating rate 300 °C/h. The optimum sintering time with respect to both templated grain growth and densification

was found to be 14 h. Two configurations of textured samples were investigated. In the planar template configuration (PTC) the tape cast plane was oriented horizontally to be parallel to the electrodes. In the vertical template configuration (VTC) the tape cast plane was oriented vertically to be perpendicular with respect to the electroded surfaces. Non-textured samples made by uniaxially pressed submicron powders were sintered together with the textured compacts.

The densities of the sintered ceramics were measured by the Archimedes' method in isopropanol (ISO 5017). X-ray diffraction (XRD) patterns were recorded for powders, templates, green tapes and sintered ceramics (D8 Focus, Bruker AXS, Karlsruhe, Germany) in Bragg-Brentano geometry. Lotgering factors[28] (F) quantifying the degree of $(00l)_{pc}$ texture were calculated from the relative peak intensities for the templates, green tapes and sintered ceramics by using the non-textured sintered ceramics as the reference. Scanning electron microscopy (SEM) was used to investigate the microstructure and morphology of submicron matrix powders, templates, green tapes and sintered bodies (S-3400N, Hitachi, Hitachi, Japan and Ultra 55, Carl Zeiss AG, Oberkochen, Germany). Piezo- and ferroelectric properties were investigated with a piezoelectric testing system (TF Analyzer 2000, aixACCT Systems GmbH, Aachen, Germany) at a frequency of 0.25 Hz and a triangular waveform. The electric field-induced strain amplitude, S_{max}, and the corresponding strain coefficient, S_{max}/E_{max}, were measured through the application of unipolar electric field cycles. Textured and non-textured KNN ceramics were cast in epoxy, polished (final grit size 1 μm) and used for electron backscatter diffraction (EBSD) investigations (SU6600, Hitachi, Hitachi, Japan). Charging was reduced by covering the samples with aluminum foil and conductive carbon paste, leaving only a small window for analysis. EBSD patterns were recorded from a sample area of 100 × 120 μm with 20 kV acceleration voltage. The patterns were indexed and analyzed

within the orthorhombic space group *Amm*2 using the EDAX OIM Data Collection and Data Analysis softwares.

2D X-ray diffraction patterns were recorded *in situ* during electric field loading at beamline 11-ID-C, Advanced Photon Source, Argonne National Laboratory. Prior to the experiment, the sintered KNN ceramics were cut into bars of approximate dimensions 1 × 1 × 10 mm, electroded with Ag-paint and annealed at 500 °C for 2 h. Diffraction patterns in the forward scattering (transmission) geometry of high energy X-rays (115 keV, wavelength 0.1081 Å) were recorded on a Perkin Elmer amorphous silicon plate detector. The experimental geometry and sample orientation is shown in Fig. 2. The azimuthal angle (γ) on the detector is defined as 0° in the horizontal direction which is transverse to the electric field, and 90° is a direction parallel to the applied electric field. The diffraction intensities measured in the vertical direction represent scattering from domains/crystallites oriented with their [*hkl*] normals approximately parallel to the electric field direction. Two configurations of the textured KNN ceramic were investigated with their grain orientation differently with respect to the detector and the applied electric field, as shown in Fig. 2. In one configuration, the TCD was oriented along the beam-detector line in the horizontal plane (PTC). In the other, the textured body was oriented with the TCD in the vertical direction (VTC). For each sample, one diffraction pattern was recorded in the unpoled state before a series of triangular electric field cycles with increasing amplitude (2.0, 2.5, 3.0 and 3.5 kV/mm) was applied. Each cycle had a period of 80 s, during which 40 diffractograms were recorded sequentially. The FIT2D software[29] was used for calibration of detector orientation and beam center position according to a CeO_2 standard[30] and extraction of γ and 2θ dependent data.[31] After the *in situ* experiments, the direct piezoelectric coefficients d_{33} of all three samples were measured with a d_{33}-meter (YE2730A, APC International Ltd., Mackeyville, PA).

For each diffractogram measured during electric field cycles, the $\{220\}_{pc}$ triplet (at $\gamma = 90°$) was fit with a Gaussian profile using MATLAB (R2012a, MathWorks INC, Natick, MA) as exemplified in Fig. 3. Constraints were applied to the peak widths in order to avoid unnatural broadening. The $\{220\}_{pc}$ group consists of three peaks that represent domain orientations with unique spontaneous polarization directions relative to the electric field direction. Peaks 1, 2 and 3 in $\{220\}_{pc}$ correspond to diffraction from the $(004)_o$, $(040)_o$ and $(222)_o$ (orthorhombic indices), respectively. The spontaneous polarization and the largest component of spontaneous strain are parallel to the longest axis in the orthorhombic unit cell ($[004]_o$), and the integrated area of peak 1 (relative to its unpoled state) is therefore used to demonstrate a changing degree of domain alignment. At $\gamma = 90°$ an increase in the area of peak 1 would indicate an increasing degree of alignment of the spontaneous strains and polarizations parallel to the electric field.[32] Peaks 2 and 3 correspond to domain orientations in which the direction of spontaneous polarization is perpendicular and ~60° to the electric field, respectively.

Results

The morphology and microstructure of the KNN templates and the submicron KNN powder are shown in the micrographs presented in Fig. 4. The powder is isometric (50-100 nm average particle size, some grains cube-shaped), while the templates exhibit a large aspect ratio (typically 20-30 μm long and 1-2 μm thick). Template alignment parallel to TCD is demonstrated in the micrograph of the green tape (Fig. 4(c)), and Fig. 4(d) demonstrates that TGG has occurred during sintering. Both the textured and the non-textured KNN materials sintered to 94 % of the theoretical density.

The development of grain texture during sintering of the tape cast materials is apparent from the XRD patterns provided in Fig. 5(a). The $\{110\}_{pc}$ reflections are the most intense in the non-textured KNN as expected if homoepitaxial growth has occurred. The X-ray diffraction patterns of the templates, the green tape (of textured material) and the textured ceramic (in the PTC configuration) demonstrate a profound enhancement of the $\{001\}_{pc}$ reflections arising from needle-like templates aligned with their long axis ($[100]_{pc}$) parallel to the tape cast plane, resulting in a Lotgering factor of 31 % for the PTC-oriented textured KNN. The diffraction patterns of the textured KNN ceramics in two different orientations (see Fig. 2), as well as of a non-textured sample are compared in Fig. 5(b). They show that the highest degree of grain orientation (F = 86 %) is parallel to the TCD, compared to normal to the tape cast plane (F = 28 %). While the main reflections in the samples can be indexed to a perovskite phase isostructural to $KNbO_3$ (PDF card 00-032-0822), small amounts of tetragonal tungsten bronze-structured secondary phase indexed to $K_2Nb_4O_{11}$ [24] is evident in some of the sintered ceramics.

Inverse pole figures generated from EBSD data (Fig. 6) display the preferential grain orientation in all directions (TD, TCD and ND) of the textured KNN material. A higher degree of preferred orientation of $<100>_{pc}$ parallel to the TCD compared to the ND and the TD is evident from the intensity of the $[100]_o$ and $[011]_o$ poles in the respective inverse pole figures. In the inverse pole figures for the TD and the ND orientations, poles corresponding to $<110>_{pc}$ directions ($[001]_o$, $[010]_o$ and $[111]_o$) are also of intensity comparable to the $<100>_{pc}$.

The polarization vs. electric field loops (Fig. 7(a)) demonstrate a lower polarization in the textured (VTC and PTC) materials compared to non-textured materials in agreement with previous observations.[42,43] The strain is higher in the VTC-textured (up to 0.06 %) compared to the non-textured materials and PTC-textured KNN (up to 0.04 %) (Fig. 7(b)). Furthermore, measurements of the unipolar normalized strain (Table II) also demonstrate that the highest strain coefficient is obtained in the VTC sample (up to 320 pm/V at 3 kV/mm). Interestingly, the strain is lower in the PTC sample (up to 140 pm/V) compared to non-textured KNN (up to 200 pm/V). Lower strain has also been observed in PTC-oriented samples of textured Mn, Ta and Li co-doped KNN compared to their non-textured counterparts.[33] These results clearly demonstrate that texture is beneficial to strain when the electric field is applied parallel to the TCD (VTC sample), but disadvantageous when the electric field is applied perpendicular to the TCD (PTC sample).

Contour plots of the $\{100\}_{pc}$ and $\{110\}_{pc}$ diffracted intensity as a function of the azimuthal angle γ recorded on the 2D detector (see Fig. 2), prior to application of electric field are shown in Fig. 8. The VTC sample shows strongly enhanced $\{100\}_{pc}$ diffraction around $\gamma = 90°$, due to the long template axis $[100]_{pc}$ oriented at $\gamma \approx 90°$. Enhanced $\{100\}_{pc}$ intensity near $\gamma = 90°$ is also observed for the PTC sample, though the intensity is distributed over a broader range of azimuthal angles, demonstrating a weaker $<100>_{pc}$ grain orientation parallel to the ND compared to the TCD. In both orientations of the textured KNN, the $\{110\}_{pc}$ reflection intensity also depends on the azimuthal angle. The maximum intensity for the VTC sample is observed around $\gamma = 45°$ and 135°, while an uneven distribution of intensity with a maximum around $\gamma = 90°$ is evident for the PTC sample. The $\{110\}_{pc}$ is the strongest reflection for the non-textured KNN and there are no significant azimuthal intensity variations, both as expected for perovskite ceramics without any grain texture.

Domain reorientation was studied by *in situ* X-ray diffraction. In all the KNN ceramics, the changes in the $\{200\}_{pc}$ reflection intensities at $\gamma = 90°$ during *in situ* electric field cycling at 3.5 kV/mm (Fig. 9) are consistent with electric field induced domain switching.[34] More specifically, the intensity of the reflection at lower 2θ angles is increased at high field amplitudes relative to the reflection at higher 2θ angles. The relative intensity changes between the two $\{200\}_{pc}$ peaks are largest for the VTC sample. Similar systematic intensity changes with electric field amplitude are also observed within other ferroelastic degenerate reflections and at other azimuthal angles. The reflections that increase or decrease in intensity depend on the azimuthal angle, which is defined as the relative angle between the different crystals and the electric field direction (Fig. 2). Nevertheless, the relative intensity changes are always largest for the VTC sample. No shift in peak positions throughout the cycles could be observed as a consequence of the low intrinsic strain in these lead-free piezoelectric ceramics.

Relative integrated intensities of the $\{220\}_{pc}$ peaks, obtained by peak fitting, are shown in Fig. 10 as a function of time during electric field loading. The relative increase in the intensity of peak 1 for the VTC sample is one order of magnitude higher compared to the other samples. The intensity of peak 1 (the $(004)_o$ reflection) increases at high field amplitudes (both for positive and negative electric fields) due to non-180° domain reorientation. When the amplitude of the field is decreased, the peak intensity decreases, likely due to back-switching of domains. The overall increase in the intensity of peak 1 throughout the cycles is attributed to a progressively increased poling state which induces a preference for domain orientations of largest d-spacing (i.e., the $[004]_o$ crystallographic direction of the orthorhombic structure).

Changes in the intensities of peaks 2 (the $(040)_o$ reflection) and 3 (the $(222)_o$ reflection) are smaller due to their crystallographic orientation (and overlap), but the peak 2 intensity appears to decrease, while the peak 3 intensity increases slightly for all samples throughout the cycles. The d_{33} measured after the *in situ* experiments was significantly higher for the VTC sample (125±3 pC/N) compared to the PTC sample (89±3 pC/N), while the non-textured material exhibited an intermediate value (107±4 pC/N). This is the same trend as for the final peak 1 intensities shown in Fig. 10 and the strain values in Fig. 7(b) and Table II.

Discussion

This work has demonstrated that alignment of needle-like KNN templates through tape casting with a gated doctor blade is a suitable method for texturing of KNN ceramics by homoepitaxial grain growth. A high degree of grain texture in the KNN ceramics was obtained parallel to the TCD, as observed by the Lotgering factors (F = 86 % parallel to TCD, F = 28 % parallel to ND), inverse pole figures, and azimuthal distribution of X-ray intensity on the 2D detector. The preferred orientation parallel to TCD originates from alignment of the needle-like templates in this direction, while the preferred orientation in the ND may be attributed to a rotational degree of freedom of the needle-like templates.

Enhanced piezoelectric response in KNN through texturing was obtained, as demonstrated by the higher values of strain (Fig. 7(b)), enhanced high-field domain reorientation (Figs. 9 and 10) and higher d_{33} of the VTC sample compared to non-textured KNN. In particular, normalized strain coefficients above 300 pm/V are significantly higher than typical values for non-textured KNN (150 pm/V[35]).

The consequences of the texture introduced by the needle-like templates are anisotropic piezoelectric and ferroelectric responses, manifested by the highest strain, d_{33} and domain reorientation parallel to TCD compared to ND. One of the origins of this anisotropic response is in the intrinsic anisotropy of the piezoelectric effect in KNN. Calculated longitudinal piezoelectric response in orthorhombic $KNbO_3$ single crystals shows a noticeable dependence on the angle from the polar axis, with the maximum response away from the polar axis.[16] This is in accordance with experimental results showing the piezoelectric constants $k_{31} = 31.2$ % and $d_{31} = 51.7$ pC/N in a $KNbO_3$ single crystal poled parallel to $[100]_{pc}$ compared to 28.9 % and 18.4 pC/N when poled parallel to $[110]_{pc}$.[17] This maximum response away from the polar axis classifies $KNbO_3$ as rotator ferroelectric. Although a similar analysis has not been provided for KNN, analogous behavior can be anticipated in ferroelectrics which are both structurally and compositionally related to $KNbO_3$. The high degree of $<100>_{pc}$ texture parallel to TCD results in few domains with their polar axis parallel to the electric field in VTC-oriented KNN ceramics. The enhanced piezoelectric response away from the polar axis observed in the VTC sample is hence in accordance with the concept of rotator-type ferroelectric behavior for orthorhombic KNN. Observation of small strain hysteresis in $<00l>_{pc}$ textured KNN has also been attributed to polarization rotation and domain engineering by Chang *et al.*[10]

In addition to the intrinsic effect as discussed above, extrinsic contributions such as domain wall motion affect the piezoelectric response. In a non-textured ceramic, non-180° domain reorientation can be restricted in some grains due to strain mismatch with the randomly oriented surrounding grains. In grain textured ceramics, alignment of spontaneous strains makes cooperative domain reorientation possible, and more complete poling and increased piezoelectric response can be obtained.[36] In the VTC sample, the electric field is applied

parallel to the direction of strongest preferred orientation, and the above mentioned mechanism for strain accommodation may explain the large increase in domain reorientation that was observed by the *in situ* XRD technique. The PTC sample also has the same strong degree of preferred orientation parallel to the TCD as the VTC sample. However, in the PTC sample the electric field is applied parallel to the ND, where the degree of grain texture is much lower than parallel to the TCD. Application of the electric field parallel to the ND breaks the symmetry of the ND and TD, and the texture symmetry becomes orthotropic (three unique and mutually perpendicular directions). The different strains in the two transverse directions (TCD and TD) interplay with the response parallel to the field direction (ND) in a way that is not yet understood. For example, domain reorientation may occur between these two transverse directions (TCD and TD) at the expense of domain reorientation into the field direction that would enhance poling or electric field-induced strain. Such strain interplay in ferroelectric orthotropic sample symmetries may explain some of the decreased piezoelectric response in the PTC sample compared to both the VTC and the non-textured sample.

Conclusion

Textured $K_{0.5}Na_{0.5}NbO_3$ (KNN) was prepared by tape casting with needle-like KNN templates using a gated doctor blade followed by homoepitaxial templated grain growth. The highest alignment (F = 86 %) of $<100>_{pc}$ was obtained parallel to the tape cast direction, while moderate (F = 28 %) $<001>_{pc}$ grain texture was obtained parallel to the tape cast plane normal. Parallel to the direction of high texture, enhanced d_{33} (125±3 pC/N), strain $((S_{max}/E_{max})_{33}$ up to 321 pm/V) and domain reorientation is observed compared to the non-textured ceramic (d_{33} = 107±4 pC/N, $(S_{max}/E_{max})_{33}$ up to 199 pm/V). The properties parallel to the direction of moderate grain texture (d_{33} = 89±3 pC/N, $(S_{max}/E_{max})_{33}$ up to 131 pm/V) are lower than both these samples. This demonstrates that texturing with needle-like KNN

templates is viable for enhancing the piezoelectric response in KNN, although requiring the alignment of the templates to be parallel to the direction of the driving electric field or mechanical force. The anisotropy in the textured KNN is explained to be consistent with enhanced piezoelectric response parallel to non-polar directions in rotator-type ferroelectrics, and different effect of strain accommodation for electric field applied parallel and perpendicular to the direction of high texture.

Acknowledgements

Financial support from NTNU and the Research Council of Norway through project number 197497/F20 «Lead-free ferro- and piezoelectric $K_{0.5}Na_{0.5}NbO_3$ -based materials» is acknowledged. Use of the Advanced Photon Source at Argonne National Laboratory was supported by the U.S. Department of Energy, Office of Science, Office of Basic Energy Sciences, under Contract No. DE-AC02-06CH11357. GT and JJ acknowledge support from the U.S. Department of the Army under Grant No. W911NF-09-1-0435. The authors would like to thank Prof. Jarle Hjelen for advice on the use of EBSD and Thanakorn Iamsasri for plotting Fig. 9.

References

1. J. Rödel, W. Jo, K. T. P. Seifert, E. M. Anton, T. Granzow, and D. Damjanovic, "Perspective on the Development of Lead-Free Piezoceramics," *J. Am. Ceram. Soc.,* **92** [6] 1153-77 (2009).
2. E. Aksel and J. L. Jones, "Advances in Lead-Free Piezoelectric Materials for Sensors and Actuators," *Sensors,* **10** [3] 1935-54 (2010).

3. S. O. Leontsev and R. E. Eitel, "Progress in Engineering High Strain Lead-Free Piezoelectric Ceramics," *Sci .Technol. Adv. Mat.,* **11** [4] 44302-15 (2010).

4. G. L. Messing, S. Trolier-McKinstry, E. M. Sabolsky, C. Duran, S. Kwon, B. Brahmaroutu, P. Park, H. Yilmaz*, et al.*, "Templated Grain Growth of Textured Piezoelectric Ceramics," *Crit. Rev. Solid State Mat. Sci.,* **29** [2] 45-96 (2004).

5. D. Damjanovic, M. Budimir, M. Davis, and N. Setter, "Piezoelectric Anisotropy: Enhanced Piezoelectric Response Along Nonpolar Directions in Perovskite Crystals," *J. Mater. Sci.,* **41** [1] 65-76 (2006).

6. M. Davis, M. Budimir, D. Damjanovic, and N. Setter, "Rotator and Extender Ferroelectrics: Importance of the Shear Coefficient to the Piezoelectric Properties of Domain-Engineered Crystals and Ceramics," *J. Appl. Phys.,* **101** [5] 054112-10 (2007).

7. Y. Saito, H. Takao, T. Tani, T. Nonoyama, K. Takatori, T. Homma, T. Nagaya, and M. Nakamura, "Lead-Free Piezoceramics," *Nature,* **432** [7013] 84-87 (2004).

8. E. Hollenstein, M. Davis, D. Damjanovic, and N. Setter, "Piezoelectric Properties of Li- and Ta-Modified $(K_{0.5}Na_{0.5})NbO_3$ Ceramics," *Appl. Phys. Lett.,* **87** [18] 182905-7 (2005).

9. T. Soller, R. Bathelt, K. Benkert, H. Bodinger, C. Schuh, and F. Schlenkrich, "Textured and Tungsten-bronze-niobate-doped (K,Na,Li)(Nb,Ta)O_3 Piezoceramic Materials," *J. Korean Phys. Soc.,* **57** [4] 942-46 (2010).

10. Y. Chang, S. Poterala, Z. Yang, and G. L. Messing, "Enhanced Electromechanical Properties and Temperature Stability of Textured $(K_{0.5}Na_{0.5})NbO_3$-based Piezoelectric Ceramics," *J. Am. Ceram. Soc.,* **94** [8] 2494-98 (2011).

11. H. Takao, Y. Saito, Y. Aoki, and K. Horibuchi, "Microstructural Evolution of Crystalline-Oriented $(K_{0.5}Na_{0.5})NbO_3$ Piezoelectric Ceramics with a Sintering Aid of CuO," *J. Am. Ceram. Soc.,* **89** [6] 1951-56 (2006).

12. Y. Chang, S. Poterala, Z. Yang, S. Trolier-McKinstry, and G. Messing, "Microstructure Development and Piezoelectric Properties of Highly Textured CuO-doped KNN by Templated Grain Growth," *J. Mater. Res.,* **25** [4] 687-94 (2010).

13. G. Tutuncu, Y. F. Chang, S. Poterala, G. L. Messing, and J. L. Jones, "In Situ Observations of Templated Grain Growth in $(Na_{0.5}K_{0.5})_{0.98}Li_{0.02}NbO_3$ Piezoceramics: Texture Development and Template-Matrix Interactions," *J. Am. Ceram. Soc.,* **95** [8] 2653-59 (2012).

14. K. Nakamura and Y. Kawamura, "Orientation Dependence of Electromechanical Coupling Factors in $KNbO_3$," *IEEE Trans. Ultrason. Ferroelectr. Freq. Control,* **47** [3] 750-55 (2000).

15. M. Zgonik, R. Schlesser, I. Biaggio, E. Voit, J. Tscherry, and P. Gunter, "Materials Constants of $KNbO_3$ Relevant for Electro- and Acousto-Optics," *J. Appl. Phys.,* **74** [2] 1287-97 (1993).

16. L. Y. Liang, Y. L. Li, S. Y. Hu, L. Q. Chen, and G. H. Lu, "Piezoelectric Anisotropy of a $KNbO_3$ Single Crystal," *J. Appl. Phys.,* **108** [9] 094111 (2010).

17. S. Wada, A. Seike, and T. Tsurumi, "Poling Treatment and Piezoelectric Properties of Potassium Niobate Ferroelectric Single Crystals," *Jpn. J. Appl. Phys. Part 1 - Regul. Pap. Short Notes Rev. Pap.,* **40** [9B] 5690-97 (2001).

18. R. E. Newnham, "Properties of Materials: Anisotropy, Symmetry, Structure.″ Oxford University Press, (2004).

19. J. F. Li, Y. H. Zhen, B. P. Zhang, L. M. Zhang, and K. Wang, "Normal Sintering of (K, Na)NbO_3-Based Lead-Free Piezoelectric Ceramics," *Ceram. Int.,* **34** [4] 783-86 (2008).

20. E. Li, R. Sasaki, T. Hoshina, H. Takeda, and T. Tsurumi, "Miniature Ultrasonic Motor Using Shear Mode of Potassium Sodium Niobate-Based Lead-Free Piezoelectric Ceramics," *Jpn. J. Appl. Phys.,* **48** [9] 09KD11 (2009).

21. J. B. Lim, S. J. Zhang, J. H. Jeon, and T. R. Shrout, "(K,Na)NbO_3-Based Ceramics for Piezoelectric "Hard"Lead-Free Materials," *J. Am. Ceram. Soc.,* **93** [5] 1218-20 (2010).

22. T. Mokkelbost, Ø. Andersen, R. A. Strøm, K. Wiik, T. Grande, and M. A. Einarsrud, "High-Temperature Proton-Conducting $LaNbO_4$-Based Materials: Powder Synthesis by Spray Pyrolysis," *J. Am. Ceram. Soc.,* **90** [11] 3395-400 (2007).

23. V. Gil, R. A. Strøm, L. J. Groven, and M.-A. Einarsrud, "$La_{28-x}W_{4+x}O_{54+3x/2}$ Powders Prepared by Spray Pyrolysis," *J. Am. Ceram. Soc.,* **95** [11] 3403-07 (2012).

24. F. Madaro, R. Sæterli, J. R. Tolchard, M.-A. Einarsrud, R. Holmestad, and T. Grande, "Molten Salt Synthesis of $K_4Nb_6O_{17}$, $K_2Nb_4O_{11}$ and KNb_3O_8 Crystals with Needle- or Plate-Like Morphology," *Crystengcomm,* **13** [5] 1304-13 (2011).

25. F. Madaro, J. R. Tolchard, Y. D. Yu, M. A. Einarsrud, and T. Grande, "Synthesis of Anisometric $KNbO_3$ and $K_{0.5}Na_{0.5}NbO_3$ Single Crystals by Chemical Conversion of Non-Perovskite Templates," *Crystengcomm,* **13** [5] 1350-59 (2011).

26. H. L. Lein, T. Tezuka, T. Grande, and M.-A. Einarsrud, "Asymmetric Proton Conducting Oxide Membranes and Fuel Cells Prepared by Aqueous Tape Casting," *Solid State Ion.,* **179** [21–26] 1146-50 (2008).

27. D.-S. Park and C.-W. Kim, "Modification of Tape Casting for Aligning the Whiskers," *J. Mater. Sci.,* **34** [23] 5827-32 (1999).

28. F. Lotgering, "Topotactical Reactions with Ferrimagnetic Oxides Having Hexagonal Crystal Structures. 1," *J. Inorg. Nucl. Chem.,* **9** [2] 113-25 (1959).

29. A. P. Hammersley, "FIT2D: An Introduction and Overview." in ESRF Internal Report. 1997.

30. A. P. Hammersley, S. O. Svensson, and A. Thompson, "Calibration and Correction of Spatial Distortions in 2D Detector Systems," *Nucl. Instrum. Meth. A*, **346** [1–2] 312-21 (1994).

31. A. P. Hammersley, S. O. Svensson, M. Hanfland, A. N. Fitch, and D. Hausermann, "Two-Dimensional Detector Software: From Real Detector to Idealised Image or Two-Theta Scan," *High Pressure Res.*, **14** [4-6] 235-48 (1996).

32. T. Iamsasri, G. Tutuncu, C. Uthaisar, S. Pojprapai, and J. Jones, "Analysis Methods for Characterizing Ferroelectric/Ferroelastic Domain Reorientation in Orthorhombic Perovskite Materials and Application to Li-doped $Na_{0.5}K_{0.5}NbO_3$," *J. Mater. Sci.*, **48** [20] 6905-10 (2013).

33. G. H. Olsen, "Texturing of Lead-Free Piezoelectric Ceramics," Master's Thesis, Norwegian University of Science and Technology (2012).

34. D. A. Hall, F. Azough, N. Middleton-Stewart, R. J. Cernik, R. Freer, T. Mori, H. Kungl, and C. Curfs, "In-situ X-ray Diffraction Study of Ferroelectric Domain Switching in Orthorhombic NKN Ceramics," *Funct. Mater. Lett.*, **3** [1] 31-34 (2010).

35. W. Jo, R. Dittmer, M. Acosta, J. Zang, C. Groh, E. Sapper, K. Wang, and J. Rödel, "Giant Electric-Field-Induced Strains in Lead-Free Ceramics for Actuator Applications - Status and Perspective," *J. Electroceram.*, **29** [1] 71-93 (2012).

36. J. L. Jones, B. J. Iverson, and K. J. Bowman, "Texture and Anisotropy of Polycrystalline Piezoelectrics," *J. Am. Ceram. Soc.*, **90** [8] 2297-314 (2007).

Tables

Table I. Starting materials for preparation of textured KNN-based piezoelectric ceramics through tape casting.

Function	Material	Supplier	Wt% in slip
Submicron powder	KNN	Synthesized in the present work	27 (90 wt% of the dry content)
Templates	KNN	Synthesized in the present work	3 (10 wt% of the dry content)
Binder	Polyvinyl alcohol (PVA) used as a 15 wt% solution in distilled water	Merck, Darmstadt, Germany	34
Plasticizer	Polyethylene glycol (PEG)	Fluka, Buchs, Germany	0.85
Defoamer	Polypropylene glycol (PPG)	Acros Organics, Geel, Belgium	0.28
Dispersant	Ammonium polymethacrylate (Darvan C)	R.T. Vanderbilt Company, Inc., Norwalk, CT	0.12
Solvent	Distilled water		36

Table II. Density (ρ), Lotgering factor (F), and unipolar piezoelectric strains $(S_{max}/E_{max})_{33}$ in the textured (VTC and PTC) and non-textured KNN.

Sample	**ρ (%)**	**F (%)**	**$(S_{max}/E_{max})_{33}$ at 2 kV/mm (pm/V)**	**$(S_{max}/E_{max})_{33}$ at 3 kV/mm (pm/V)**
VTC-KNN	94	86	282±1	321±1
KNN	94	-	183±3	199±3
PTC-KNN	94	28	120±5	131±1

Figure captions

Fig. 1. Alignment procedure for KNN needle like templates in KNN matrix during tape casting and crystallographic orientation of templates. ND, TD and TCD are the normal, transverse and tape casting directions, respectively.

Fig. 2. Experimental setup for *in situ* electric field diffraction of KNN recorded on a 2D detector at the Advanced Photon Source. The azimuthal angle (γ) is defined as 0° in the horizontal direction. Inset: the two investigated orientations of the textured KNN ceramics.

Fig. 3. Example of peak fitting of the $\{220\}_{pc}$ in KNN with three Gaussian peaks including the difference curve (data-fit).

Fig. 4. SEM images of KNN materials. (a) KNN needle-like templates used for tape casting, (b) KNN submicron matrix powder for tape casting, (c) green tape with oriented KNN template in KNN matrix after tape casting, and (d) sintered compact of textured KNN. The sample orientation in (c) and (d) is indicated with the displayed axes; ND is pointing out of the image plane.

Fig. 5. XRD patterns from (a) KNN materials at different stages of the texturing process, taken in the Bragg-Brentano geometry from the horizontal surface in the PTC configuration. (b) XRD patterns in the forward scattering geometry for the PTC- and VTC-textured, and non-textured KNN ceramics. The diffractograms are extracted at $\gamma = 90°$ on a 2D detector (according to Fig. 2) and the diffracting planes are indicated for clarity. All diffractograms in (a) and (b) are normalized on the most intense reflection. * indicates a tetragonal tungsten bronze-structured secondary phase.

Fig. 6. Inverse pole figures for textured KNN in orthorhombic indices obtained using EBSD. The intensity is in units of multiplies of random distribution (mrd) as indicated by the

colorbar. The two quadrants of the inverse pole figures are shown although they should be symmetrically equivalent.

Fig. 7. (a) Polarization and (b) strain vs. electric field for textured (PTC and VTC) and non-textured KNN.

Fig. 8. Contour plots of diffracted intensity vs. azimuthal angle (γ) for textured (PTC and VTC) and non-textured KNN. Each plot uses a separate z-axis, as indicated by the colorbar to the right of each plot.

Fig. 9. Surface and contour plots of the diffracted $\{200\}_{pc}$ of KNN during *in situ* electric field loading. $(002)_{pc}$ is at ~3.10° and $(200)_{pc}$ at ~3.14° 2θ. (a) VTC, (b) PTC and (c) non-textured.

Fig. 10. Integrated intensity of $\{220\}_{pc}$ peak 1 relative to its non-poled integrated intensity measured *in situ* for each orientation of KNN vs. the sequence of electric field cycles.

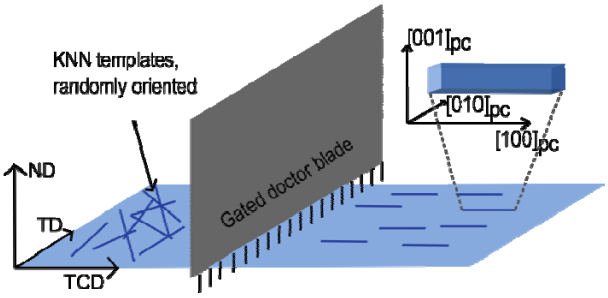

Fig. 1. Alignment procedure for KNN needle like templates in KNN matrix during tape casting and crystallographic orientation of templates. ND, TD and TCD are the normal, transverse and tape casting directions, respectively.

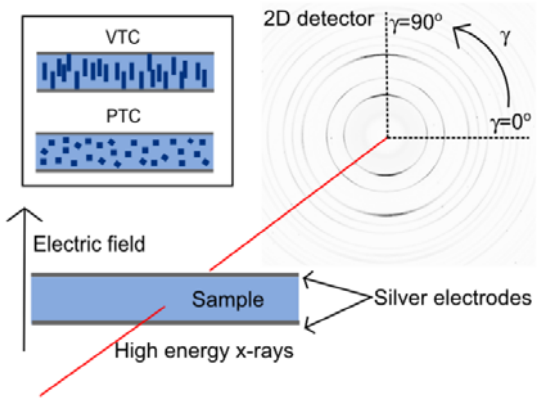

Fig. 2. Experimental setup for *in situ* electric field diffraction of KNN recorded on a 2D detector at the Advanced Photon Source. The azimuthal angle (γ) is defined as 0° in the horizontal direction. Inset: the two investigated orientations of the textured KNN ceramics.

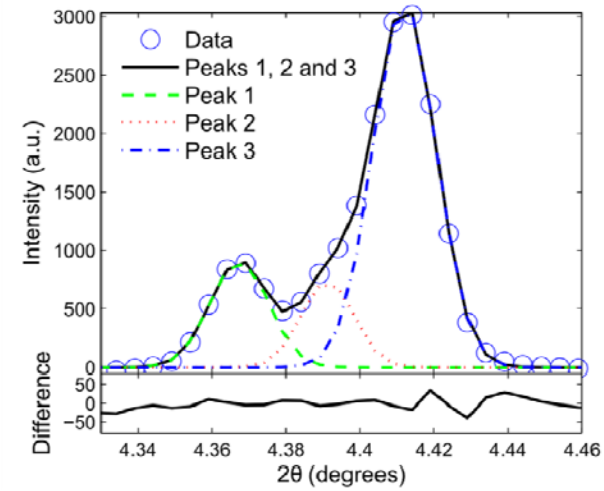

Fig. 3. Example of peak fitting of the $\{220\}_{pc}$ in KNN with three Gaussian peaks including the difference curve (data-fit).

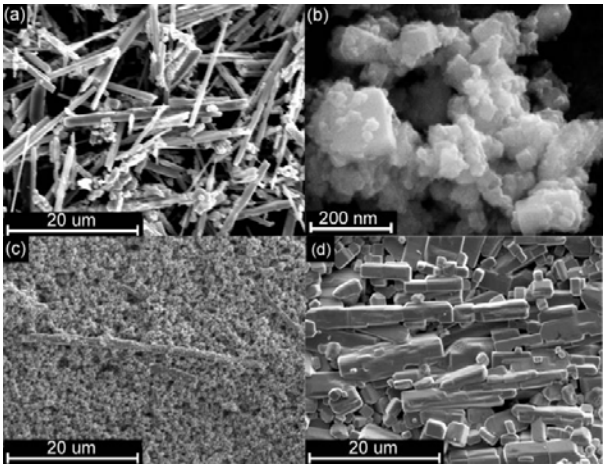

Fig. 4. SEM images of KNN materials. (a) KNN needle-like templates used for tape casting, (b) KNN submicron matrix powder for tape casting, (c) top-view of green tape with oriented KNN template in KNN matrix after tape casting (TCD is horizontal) and (d) top-view of sintered compact of textured KNN (TCD is horizontal).

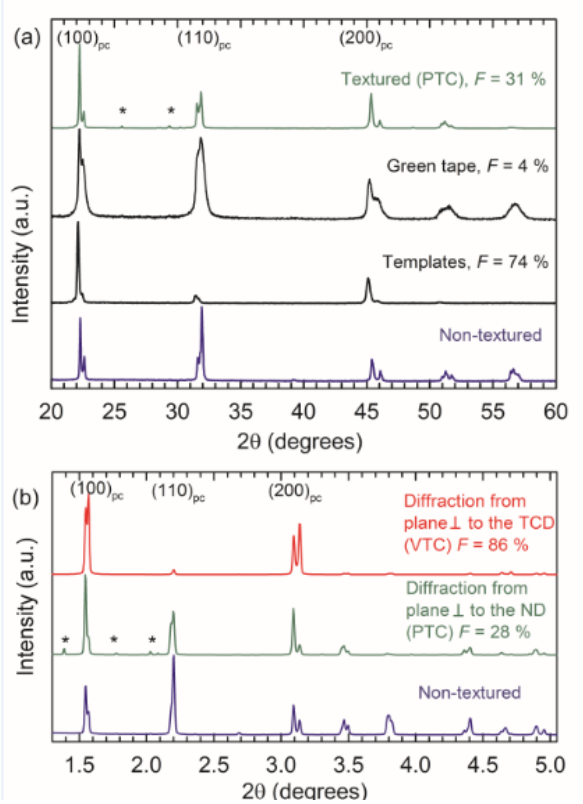

Fig. 5. XRD patterns from (a) KNN materials at different stages of the texturing process, taken in the Bragg-Brentano geometry from the horizontal surface in the PTC configuration. (b) XRD patterns in the forward scattering geometry for the PTC- and VTC-textured, and non-textured KNN ceramics. The diffractograms are extracted at $\gamma = 90°$ on a 2D detector (according to Fig. 2) and the diffracting planes are indicated for clarity. All diffractograms in (a) and (b) are normalized on the most intense reflection. * indicates a tetragonal tungsten bronze-structured secondary phase.

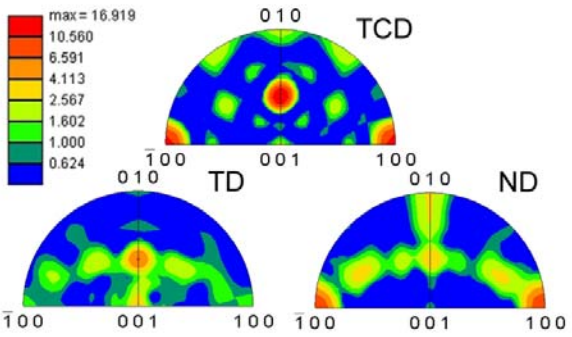

Fig. 6. Inverse pole figures for textured KNN in orthorhombic indices obtained using EBSD. The intensity is in units of multiplies of random distribution (mrd) as indicated by the colorbar. The two quadrants of the inverse pole figures are shown although they should be symmetrically equivalent.

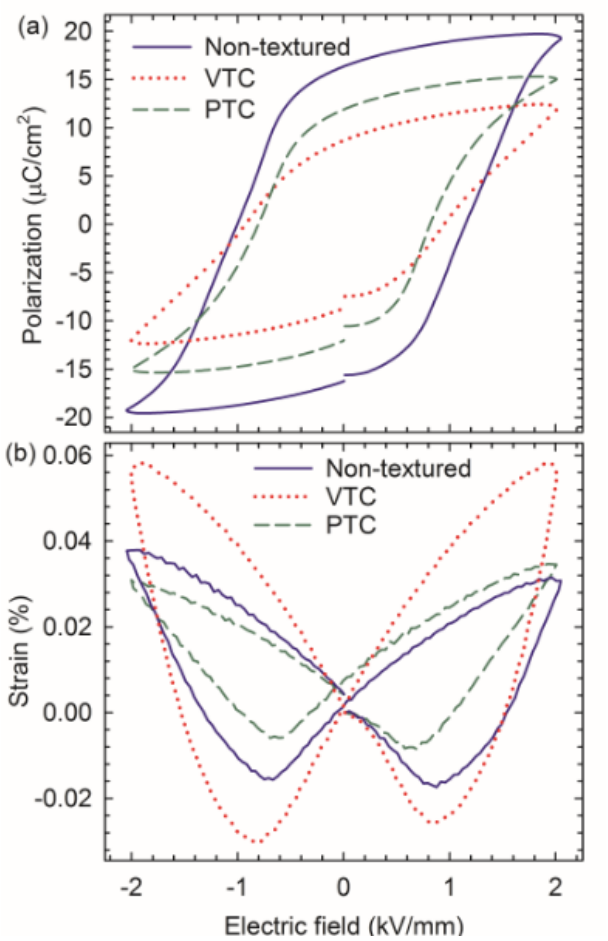

Fig. 7. (a) Polarization and (b) strain vs. electric field for textured (PTC and VTC) and non-textured KNN.

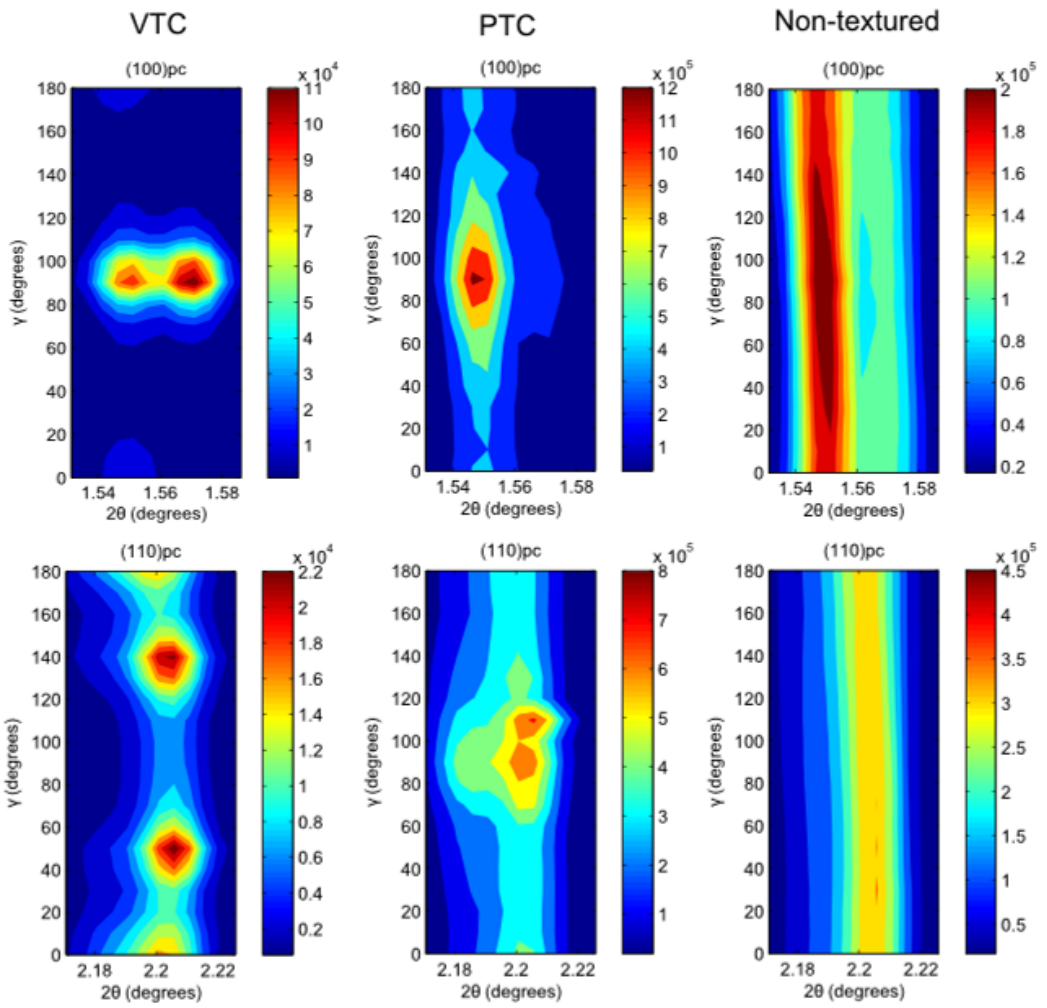

Fig. 8. Contour plots of diffracted intensity vs. azimuthal angle (γ) for textured (PTC and VTC) and non-textured KNN. Each plot uses a separate z-axis, as indicated by the colorbar to the right of each plot.

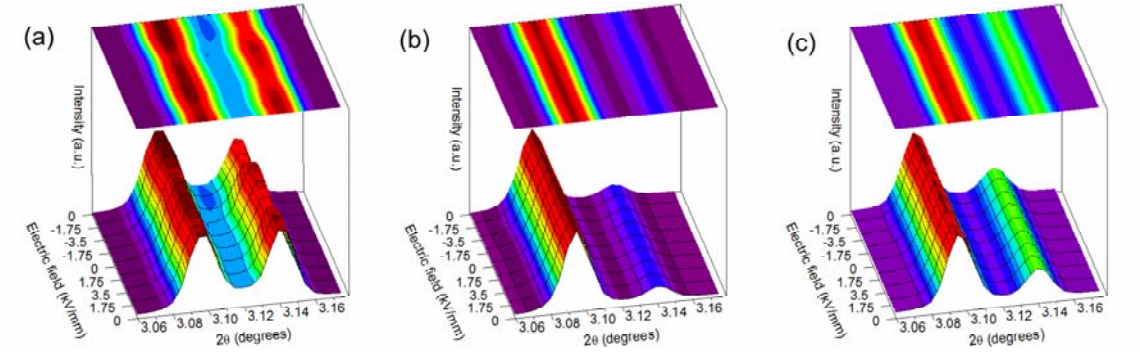

Fig. 9. Surface and contour plots of the diffracted $\{200\}_{pc}$ of KNN during *in situ* electric field loading. $(002)_{pc}$ is at ~3.10° and $(200)_{pc}$ at ~3.14° 2θ. (a) VTC, (b) PTC and (c) non-textured.

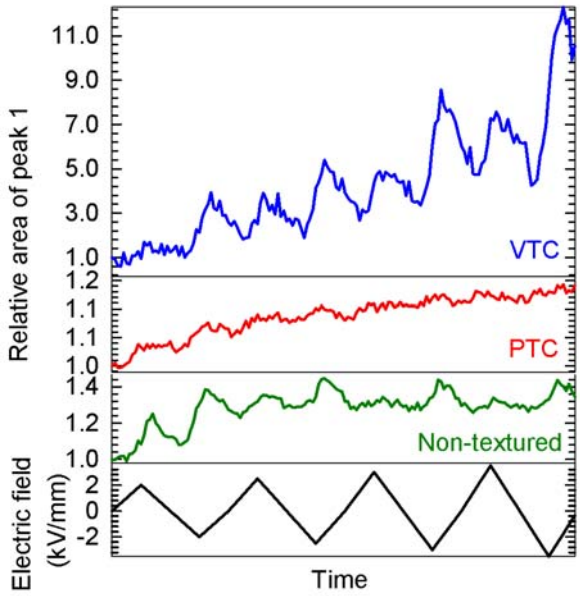

Fig. 10. Integrated intensity of $\{220\}_{pc}$ peak 1 relative to its non-poled integrated intensity measured *in situ* for each orientation of KNN vs. the sequence of electric field cycles.